Eidgenössische Technische Hochschule Zürich
Swiss Federal Institute of Technology Zurich

Design of a superconducting magnetic shield

An experimental semester thesis performed at the Quantum Device Laboratory

Jonas Krieger

ETH Zurich, 2014-2015

Supervisor: M. Oppliger
Handed-in to: Prof. Dr. A. Wallraff

Abstract

To prohibit that external magnetic fields influence a transmon qubit, a superconducting magnetic shield and a cap have been designed and fabricated out of aluminium. The effects of this shield in comparison to the already existing cryoperm shield have been studied in a finite element analysis simulation. This simulation predicts an improvement of the shielding properties by a factor of 500. However in measurements no effect of the new shield on the properties of the qubit could be confirmed. This might imply that at the time the shielded external magnetic fluctuations are not limiting the performance of the qubit.

Contents

1. Introduction

In classical electronics information is stored in bits, which are two level classical systems with states 0 and 1. A two level quantum mechanical system can also be used to process information. Such systems are called qubits. But while a classical bit is in a distinct state at every time, a qubit can be in an arbitrary superposition of its two states. This fact allows to write algorithms which are faster than the corresponding classical algorithms. For example the quantum search algorithm developed by Grover et al. [1] requires only $O(\sqrt{N})$ steps instead of $O(N)$ in a classical computer.

A possible way to construct a qubit using Josephson junctions is the transmon [2]. It consists of a superconducting loop interrupted by two insulating tunnel barriers. One parameter to control the properties of the qubit is the magnetic flux through this loop. However to allow a stable operation of the qubit it is important to minimize the noise in this magnetic flux.

Until now external magnetic fields have been shielded by a cryoperm magnetic shield. Note that cryoperm is a soft ferromagnetic material with a high permeability which diverts external magnetic fields into the shield [3]. It would also be possible to construct a shield out of a diamagnetic material, which expels applied magnetic fields. A bulk superconductor in the Meissner state is a perfect diamagnet [4].[1] The aim of this thesis was therefore to examine first in a simulation and afterwards in the experiment whether such a superconducting magnetic shield can improve the operation of the qubit.

In the following first the theory of the transmon qubit and of microwave transmission lines will be introduced. Then the results of the simulation will be presented and the design of the superconducting magnetic shield will be shown. Afterwards the measurement techniques will be explained. Finally the results are presented and the conclusions are drawn. In addition there is an appendix showing some new designs for printed circuit boards and corresponding covers.

[1] @ Markus: Should I rather cite Meissner and Ochsenfeld here?

2. Theory

2.1. Qubit

Consider a qubit with a ground state $|g\rangle$ and an excited state $|e\rangle$ with an energy difference $h\nu_{\text{qubit}}$. In generally its wavefunction $|\psi\rangle$ will be a superposition of these two energy eigenstates

$$|\psi\rangle = a\,|g\rangle + b\,|e\rangle\,, \tag{1}$$

where $|a|^2+|b|^2 = 1$. A possible implementation of a qubit is to use a special arrangement of superconductors separated by an insulating tunnel barrier. The functional principle of this transmon qubit is explained in the following.

2.1.1. Josephson effect

A Josephson junction consists of two superconductors, separated by a thin insulating layer. The Cooper pairs may tunnel from one superconductor to the other. Now a gate voltage V can be applied on the junction (by capacitively coupling it to one of the superconductors), as it is done in the Cooper pair box, see Fig. 1. In Ginzburg-Landau theory the order parameter of the superconductors can be described by [4] $\psi_j = \sqrt{n_j}e^{i\varphi_j}$, where n_j denote the densities of the Cooper pairs and φ_j are complex phases, $j = 1, 2$. Assuming the energy is set to zero symmetrically in the barrier [5] the system is described by

$$i\hbar\dot{\Psi}_{1,2} = \pm eV\Psi_{1,2} + T\Psi_{2,1},$$

where T characterizes the tunnelling and e is the charge of an electron. Inserting the expression above this solves to $\dot{n}_1 = -\dot{n}_2 \propto \sin(\varphi_2 - \varphi_1)$, $\hbar(\dot{\varphi}_2 - \dot{\varphi}_1) = -2eV$. Integrating the second equation gives the current across the junction

$$I \propto \dot{n}_1 \propto \sin\left(\frac{2eV}{\hbar}t + \Delta\varphi\right).$$

The time dependent term in the sine function is called AC Josephson effect, whereas the constant is called DC Josephson effect [6].

2.1.2. Cooper pair box

A Cooper pair box (CPB) consists of a superconducting island connected to a superconducting reservoir via a Josephson junction and to a gate voltage V via a capacitance C_{g} [8]. A schematic of a Cooper pair box is shown in Fig. 1. Assuming all electrons in the island are paired, the only remaining degree of freedom is the number of excess Cooper pairs n[2] [9]. This number has to be treated quantum mechanically. Let $\hat{n}$ be

[2] $n = 0$ corresponds to a electrically neutral island.

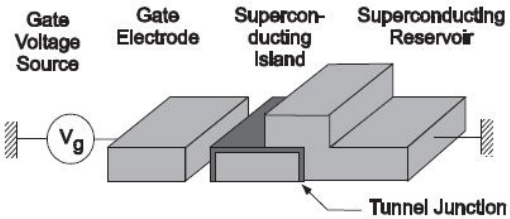

Figure 1: Schematic drawing of a Cooper pair box, from [7]

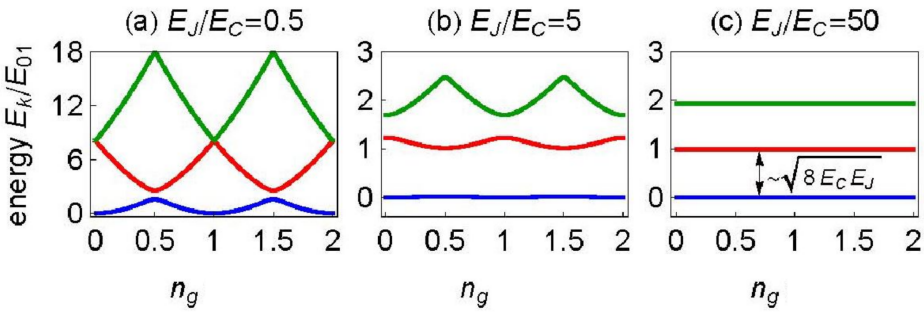

Figure 2: Energy levels of the CPB for different $E_\mathrm{J}/E_\mathrm{C}$ as a function of the number of Cooper pairs induced by the gate voltage, from [10].

the corresponding operator with eigenvalues n and eigenvectors $|n\rangle$. Then the system is described by the Hamiltonian

$$H_\mathrm{CPB} = \sum_n \left[E_\mathrm{C} \left(\hat{n} - n_g\right)^2 |n\rangle \langle n| - \frac{E_\mathrm{J}}{2} \left(|n\rangle \langle n+1| + |n+1\rangle \langle n| \right) \right], \tag{2}$$

as derived in [7].

The first term describes the electrostatic energy of the excess Cooper pairs, where $E_\mathrm{C} = \frac{(2e)^2}{2C_\mathrm{tot}}$ is the energy needed to add a single electron to the junction, $n_g = \frac{C_g V}{2e}$ is the number of Cooper pairs induced by the gate voltage, if there would be no tunnelling and C_tot is the total capacity of the system. The second term describes the tunnelling across the junction, where E_J is the Josephson energy.

The energy levels of the Hamiltonian in Eq. (2) are shown in Fig. 2.

2.1.3. Split Cooper pair box

If the superconducting island of the Cooper pair box is connected to the reservoir via two Josephson junctions (as shown in Fig 3), a superconducting loop is formed. An

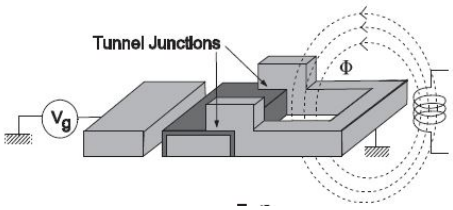

Figure 3: Schematic drawing of a split Cooper pair box with a gate voltage V_g and a flux Phi through the loop [7]

external magnetic flux Φ can be applied through this loop. Using flux quantization in the superconductor and assuming a symmetrical junctions ($E_{\mathrm{J1}} = E_{\mathrm{J2}}$) it can be shown [6, 8] that this modifies the Josephson energy in the Hamiltonian in Eq. (2):

$$E_{\mathrm{J}} \rightarrow (E_{\mathrm{J1}} + E_{\mathrm{J2}}) \cos\left(\frac{\pi\Phi}{\Phi_0}\right), \tag{3}$$

where $E_{\mathrm{J1}}, E_{\mathrm{J2}}$ are the Josephson energies of the two junctions and $\Phi_0 = \frac{h}{2e}$ is the superconducting flux quantum. Note that by using a split Cooper pair box it is possible to tune the ratio of $E_{\mathrm{J}}/E_{\mathrm{C}}$ (see Fig. 2), which was determined by fabrication properties for the Cooper pair box.

To use this split Cooper pair box as a qubit, it has to be modelled as a two level system. The two lowest energy levels will be the states $|g\rangle$ and $|e\rangle$. It can be seen from Fig. 2 that for $E_{\mathrm{J}} \approx E_{\mathrm{C}}$ the energy difference of the two levels strongly depends on the gate voltage. But in an ideal quantum mechanical two level system, the two levels have a fixed energy difference. The noise in the gate voltage will therefore destroy the qubit behaviour.

Consider the case where $E_{\mathrm{J}} \gg E_{\mathrm{C}}$ such that the first term in equation 2 can be neglected. In this case there is no dependence on the gate voltage. The system has well defined energy levels. But these levels are equally spaced, as for the quantum harmonic oscillator. It is no more possible to excite a transition to the first energy level without exciting the others too. It is therefore not possible to correctly model this case with only two levels.

In between where $E_{\mathrm{J}}/E_{\mathrm{C}} \approx 100$ the sensitivity to charge noise is small enough and the anharmonicity is big enough to treat the system as a qubit. In this regime the split Cooper pair box is called transmon [6].

2.2. Decoherence

To perform a quantum computing algorithm, the qubit has to ideally stay in a prepared state until it is measured. When designing a quantum computing experiment it is therefore necessary to minimize all external sources of decoherence, which may change the

state of the qubit by coupling to the environment. Suppose the qubit is in its excited energy eigenstate $|e\rangle$. Then the coupling to the environment will cause decay into the ground state with a rate $\Gamma_\downarrow \approx \frac{1}{T_1}$. This process is called energy relaxation and T_1 is the corresponding energy relaxation time[3].

But in general the qubit is in a superposition state. It is useful to reparametrize the wavefunction Eq. (1) of such a state by choosing the phase of $|\psi\rangle$ such that the parameter a is real:

$$|\psi\rangle = \cos\vartheta\,|g\rangle + e^{i\varphi}\sin\vartheta\,|e\rangle\,, \quad \text{where} \quad \vartheta \in \left[0, \frac{\pi}{2}\right], \varphi \in [0, 2\pi]. \tag{4}$$

The energy relaxation destroys the knowledge of ϑ in Eq. (4). There can also be a loss of information on φ due to coupling to the environment. This process is called dephasing. The corresponding dephasing rate is given by $\Gamma_2 = \frac{\Gamma_1}{2} + \Gamma_\Phi$. Here the first term describes the dephasing of the qubit due to energy relaxation and the second term describes a pure dephasing. A pure dephasing may arise, if the energy difference of the two qubit states is changed by noise, which leads to the accumulation of a random phase [6]. In an experiment normally the dephasing time $T_2 = \frac{1}{\Gamma_2}$ is measured.
A qubit in a experiment always couples to the environment. In fact it has to, because otherwise it could not be manipulated and measured. There are different external sources of decoherence which may change the state of a transmon, for example charge noise at the gate voltage capacitor, flux noise through the superconducting loop, resistive losses in the Cooper pair box and other mechanisms. All these are described in [8] in detail.

2.2.1. Flux noise

The purpose of the superconducting shield constructed as a part of this thesis is to expel the external magnetic fields. To understand how these can cause a decoherence of the transmon, the associated mechanisms are here discussed, closely following the treatment in [8].

To see the effect of flux noise lets consider a perturbation $\delta\Phi$ of the flux through the superconducting loop. The Hamiltonian of the transmon given by Eq. (2) in combination with Eq. (3) can be expanded in first order around Φ. Considering only the two lowest levels this gives a perturbation Hamiltonian

$$\hat{\xi}_\Phi = \delta\Phi \frac{\pi}{2\Phi_0}(E_{J1} + E_{J2}) \sin\left(\frac{\pi\Phi}{\Phi_0}\right)(|1\rangle\langle 0| + |0\rangle\langle 1|)\,.$$

The transition rate can now be calculated from Fermi's Golden Rule.

$$\Gamma_\downarrow = \frac{1}{\hbar^2}\left|\langle g|\,\hat{\xi}_\Phi\,|e\rangle\right|^2 S_\Phi(\omega)$$

[3] In fact $T_1 = \frac{1}{\Gamma_1} := \frac{1}{\Gamma_\uparrow + \Gamma_\downarrow}$, where $\Gamma_\uparrow$ is the rate of an excitement from $|g\rangle$ to $|e\rangle$ [8], but at very low temperature there is not enough energy to thermally excite the system ($k_B T \ll h\nu_{\text{qubit}}$), so $\Gamma_\uparrow \ll \Gamma_\downarrow$.

Here $S_\Phi(\omega)$ denotes the spectral density of the bath flux noise, see [8]. Note that from Eq. (2) it follows that, at $n_g = 1$, $|e\rangle$ and $|g\rangle$ are eigenstates of $\hat{\xi}_\Phi$ and therefore at this point there is no first order dependence of $\Gamma_\downarrow$ on the flux noise[4]. At this so called sweet spot ($n_g = 1$) the matrix element for the charge noise is minimized, too [8].

Thus the flux noise will primarily have an effect on T_2. At $n_g = 1$ the dephasing rate caused by a flux noise with a standard deviation of σ_Φ is given by [8]:

$$\Gamma_2^\Phi = \frac{\pi^2 \sigma_\Phi^2}{\Phi_0^2} 2\pi\nu_{\text{qubit}}.$$

2.3. Measurement set-up and Microwave guides

In analogy to a cavity quantum electrodynamics experiment where a two level atom in an optical cavity strongly interacts with the photons in this cavity (see for example [11]), a transmon can be put into a microwave line resonator. There it will interact with the quantized electromagnetic field in the cavity. If the transmon transition frequency is the same as the resonator frequency, the first energy eigenstate of this system will be a superposition of a photon in the resonator with the qubit in the ground state and of an empty resonator with a excited qubit. If the frequencies do not match the effective transition frequency of the transmon will still be shifted. The description of this geometry is called circuit quantum electrodynamics (CQED). A detailed overview of CQED can be found in [8]. Several such qubits in resonators are printed on a chip [12], which then is mounted on a printed circuit board (PCB). The photon flux through the resonator and the gate voltage of the qubit are controlled by microwaves, whereas the flux through the superconducting loop is regulated by using coils, which are placed below the PCB. The whole experiment is then placed in a dilution refrigerator and cooled down to 20 $mathrm\ mK$ such that $k_\text{B}T \ll h\nu_{\text{qubit}}$ [12].

2.3.1. Transmission lines

The microwaves are guided to the PCB by coaxial cables. On the PCB the chip is wired to the connection of these cables by conductor baked coplanar waveguides. A simplified model of such a waveguide is that of the transmission line:

In principle a transmission line can be thought to consist of at least two conductors[5], between which electromagnetic waves can propagate. Its behaviour can be modelled by a lumped element circuit, assigning to every infinitesimal piece of length Δz of the transmission line a resistance $\frac{\mathrm{d}R}{\mathrm{d}z}\Delta z$ and a inductance $\frac{\mathrm{d}L}{\mathrm{d}z}\Delta z$ as well as a capacitance $\frac{\mathrm{d}C}{\mathrm{d}z}\Delta z$ and a shunt conductance $\frac{\mathrm{d}G}{\mathrm{d}z}\Delta z$ between the conductors. A schematic picture of the lumped element circuit can be seen in Fig. 4. Applying Kirchhoff's laws and

[4] This is only true under the assumption that $E_{J1} = E_{J2}$. For a full treatment see [8]

[5] One conductor can not support TEM waves as shown in [13].

solving for propagating wave solutions with angular frequency ω the voltage $v(z,t)$ and the current $i(z,t)$ through the transmission line resolves to be

$$v(z,t) = |V_0^+| \cos(\omega t - \beta z + \phi^+) e^{-\alpha z} + |V_0^-| \cos(\omega t + \beta z + \phi^-) e^{\alpha z}$$
$$i(z,t) = \left|\frac{V_0^+}{Z_0}\right| \cos(\omega t - \beta z + \phi_i^+) e^{-\alpha z} - \left|\frac{V_0^-}{Z_0}\right| \cos(\omega t + \beta z + \phi_i^-) e^{\alpha z},$$

where

$$Z_0 = \frac{\frac{\mathrm{d}R}{\mathrm{d}z} + i\omega\frac{\mathrm{d}L}{\mathrm{d}z}}{\gamma}$$

is the characteristic impedance, which describes the (complex) ratio of voltage to current, and

$$\gamma = \alpha + i\beta = \sqrt{\left(\frac{\mathrm{d}R}{\mathrm{d}z} + i\omega\frac{\mathrm{d}L}{\mathrm{d}z}\right)\left(\frac{\mathrm{d}G}{\mathrm{d}z} + i\omega\frac{\mathrm{d}C}{\mathrm{d}z}\right)}.$$

Here the parameters α and β are the real and imaginary part of γ, respectively. The calculations can be found in [13, 14] .

Suppose a transmission line with impedance Z_0 is terminated with a load $Z_L \neq Z_0$ (e.g. connected to another transmission line with impedance Z_L). Then an incoming wave of the form $V_0^+ e^{-i\beta z}$ will generate a reflected wave $V_0^- e^{i\beta z}$ with $V_0^- = \frac{Z_L - Z_0}{Z_L + Z_0} V_0^+$ to satisfy the voltage to current ratio at the transition[6]. Sometimes these reflections are undesirable, for example at the interface of the PCB and the chip, or at the connection of the coax cable to the PCB. Therefore it is important to match the impedance of all the different waveguides.

2.3.2. Conductor baked coplanar waveguide

A conductor baked coplanar waveguide (CBCPW) consists of a dielectric material of thickness h and dielectric constant ε_r which is enclosed by a grounded bottom and top conducting plane. In the top plane, there are two gaps of width W around a centre pin of width $\frac{a}{2}$. This centre pin has not a fixed potential, which allows electromagnetic waves to travel along this waveguide.

To calculate the characteristic impedance of a CBCPW, note that in general the impedance of a waveguide can be calculated by solving Maxwell's Equations with boundary conditions at the conductors. For a CBCPW [15] this evaluates to:

$$Z_0 = \frac{60\pi}{\varepsilon_\mathrm{eff}} \frac{1}{\frac{K(k)}{K(k')} + \frac{K(k_3)}{K(k_3')}}$$

[6] It can be assumed that the transition is at $z = 0$ such that the condition on V_0^- follows from $Z_L = \frac{V(0)}{I(0)} = \frac{V_0^+ + V_0^-}{V_0^+ - V_0^-} Z_0$. see [13]

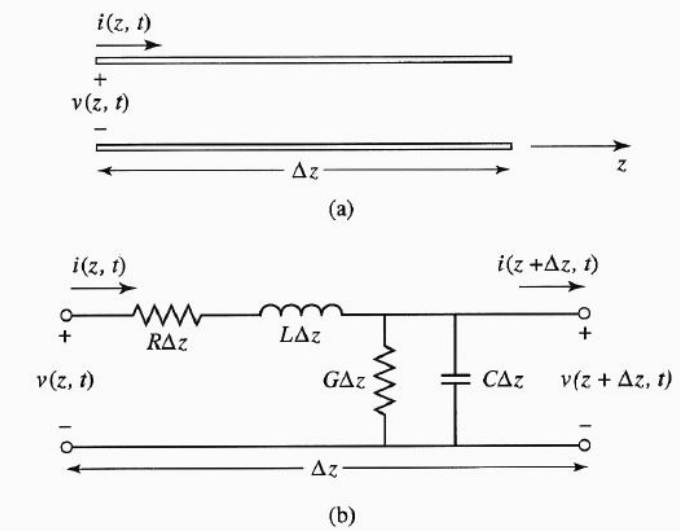

Figure 4: Schematic drawing of transmission line and its model as a lumped element circuit, from [13].

where

$$\varepsilon_{\text{eff}} = \frac{1 + \varepsilon_{\text{r}} \frac{K(k')K(k_3)}{K(k)K(k_3')}}{1 + \frac{K(k')K(k_3)}{K(k)K(k_3')}}, \qquad K(k) := \int_0^{\frac{\pi}{2}} \frac{\mathrm{d}\theta}{\sqrt{1 - k^2 \sin^2\theta}}$$

$$k = \frac{a}{b}, \qquad k_3 = \frac{\tanh\left(\frac{\pi a}{2h}\right)}{\tanh\left(\frac{\pi b}{2h}\right)},$$

$$k' = \sqrt{1 - k^2}, \qquad \text{and } k_3' = \sqrt{1 - k_3^2}.$$

Above $K(k)$ is the complete elliptic integral of the first kind.

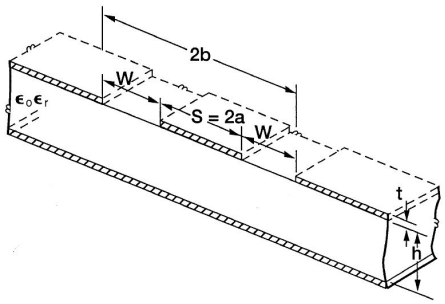

Figure 5: A conductor baked coplanar waveguide, from [15].

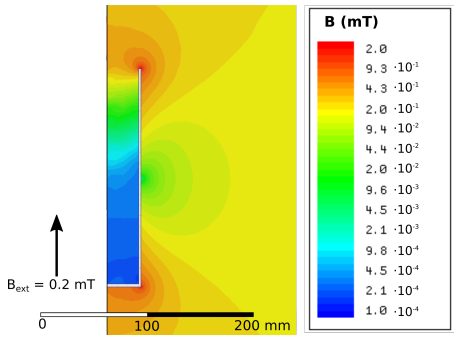

Figure 6: Simulated magnitude of the magnetic field while using only the cryoperm shield. Note that only a part of the simulated volume is shown.

3. Simulations

The already existing cryoperm magnetic shield is a hollow cylinder with one open side which is put over the qubit. To check how well it excludes external magnetic fields and whether there would be an improvement from using an additional superconducting shield, numerical simulations were performed with the commercial software *Ansoft Maxwell 14*. This is a tool which uses a finite element analysis method to iteratively solve the magnetostatic Maxwell's equations under user defined boundary conditions. Because the problem is cylindrically symmetric only a half-plane has been simulated. A cylinder with a diameter and a height of 1 m containing vacuum has been chosen as a total volume for the simulation. Boundary conditions corresponding to an external magnetic field of 0.2 mT along the cylinder axis were added to the surface of this cylinder.

Such an external magnetic field B can induce a magnetisation M into a medium placed into this field. This is usually described by the magnetic field strength $H = \frac{B}{\mu_0} - M$, where μ_0 is the permeability of the vacuum. This can be reformulated into $B = \mu\mu_0 H$ by using the relative permeability μ. To model the cryoperm shield a pre-implemented $\mu(B)$ dependence was used. A superconductor in the Meissner state has $\mu = 0$. In the simulation this was approximated by using $\mu = 10^{-5}$.

The simulation with only a cryoperm shield is shown in figure 6. As expected for a ferromagnetic material which has a magnetisation parallel to the applied field the field at the bottom of the shield is higher and the field at the side is lower than the external magnetic field. The largest fields are found at the edges. From the opening at the top of the shield to its bottom the magnetic field drops by almost three orders of magnitude.

3.1. Results of the Simulation

Several different arrangements of superconducting and cryoperm shields were examined. Of course a perfect shielding could be achieved by covering the whole qubit with the

superconductor. But this is not possible as there are several cables which have to leave through the shield. It was therefore tried to use a superconducting shield in the same shape as the cryoperm together with a superconducting cap. It was tried whether it is better to place the superconducting shield inside or outside of the cryoperm. The corresponding simulations without caps are shown in figure 7. Note that as before in both cases the magnitude of the field near the edges of the outer cylinders is bigger than the applied external field.

The different magnetic respond of the two materials is most clearly seen when looking at the bottom face of the outer shield. In figure 7 a) the field below the cryoperm shield is again bigger than the external field. However the superconductor in figure 7 b) shows the opposite behaviour. Something similar happens at the upper edge of the shield. Note that if the cryoperm is on the outside there is a region above the shield where the magnitude of the magnetic field is larger than the external field. This region is not present when placing the superconductor outside. This could explain why the shielding is better in the latter case.

The cap was placed at a variable height h above the shields and its diameter was varied from $0.5 \cdot D_{\mathrm{S}}$ to $2 \cdot D_{\mathrm{S}}$, where D_{S} is the diameter of the outer shield. Some of these simulations are shown in figure 8. Note that the main effect of the cap is that it further decreases the area where the fields can penetrate into the shield. If this area is small enough the field is attenuated already at the top of the shield. For example in figure 8 c) the field at the opening of the inner cryoperm shield is almost an order of magnitude smaller than the external field.

The improvement in the shielding was measured quantitatively by looking at the magnitude of the magnetic field at the position of the qubit. In figure 9 this quantity is shown for all the performed simulations. Based on this it was decided to build a superconducting shield and a cap with the same diameter and place them outside of the cryoperm.

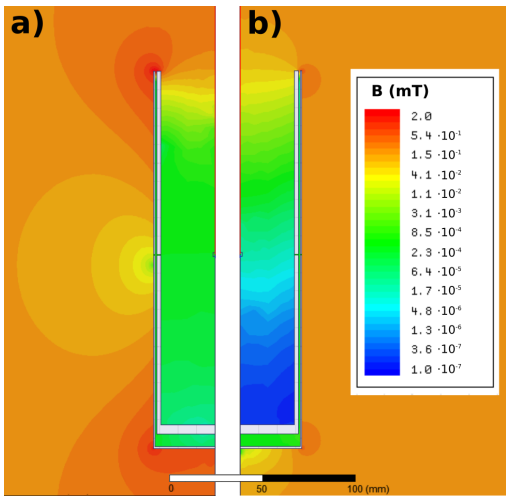

Figure 7: Simulated magnitude of the magnetic field for an external magnetic field of 0.2 mT. In **a)** the superconducting shield is placed inside of the cryoperm. In **b)** it is vice versa.

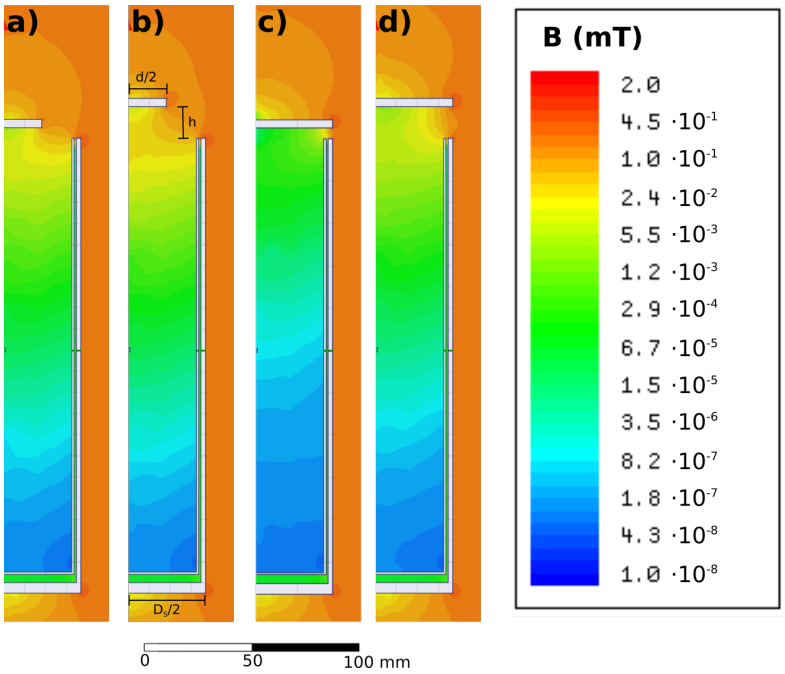

Figure 8: Simulated magnitude of the magnetic field for an external magnetic field of 0.2 mT for different cap heights h and cap sizes d as indicated in **b)**. In **a)** $d = 0.5D_S$ and $h = 5$ mm. In **b)** $d = 0.5D_S$ and $h = 15$ mm. In **c)** $d = D_S$ and $h = 5$ mm. Finally in **d)** $d = D_S$ and $h = 15$ mm.

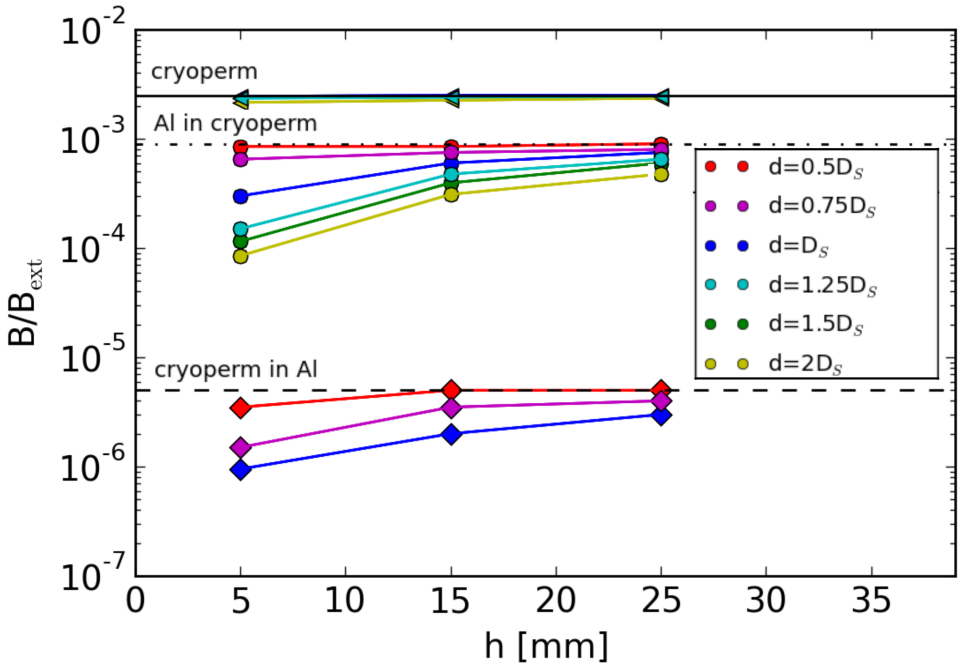

Figure 9: Attenuation of the magnetic field as a function of the cap height above the shields for three different arrangements of the shields. The solid line and the left facing triangles correspond to the situation where only the cryoperm was used. The dashed-dotted line and the circles show the results for the superconductor inside of the cryoperm and the dashed line as well as the diamond markers show the results for the superconductor outside of the cryoperm. The cap diameter d is encoded in colour. The lines show the attenuation when no cap is used.

Figure 10: Photo of the aluminium shield.

4. Superconducting shield

As a material for the superconducting shield it was decided to use aluminium (specification: EN AW-6082), which is a conventional type I superconductor with a transition temperature of 1.18 K [16]. The shield and the cap were designed in the commercial CAD-software *Autodesk Inventor Professional 2014* and produced by the workshop. Photos of the shield and the cap are shown in the figures 10 and 11, respectively. Note that the four small holes in the shield contain a screw thread which allows the shield to be screwed to a cross-piece. In the cap there is a hole in the middle, such that it can be screwed to the cryostat. In addition there are several slots at the edge to allow the cables to come out. Finally in figure 12 there is a photo of the shield as it is mounted onto the cryostat. Note that in the end there was not enough time to also install the cap. It would have made a rearrangement of all the cables necessary.

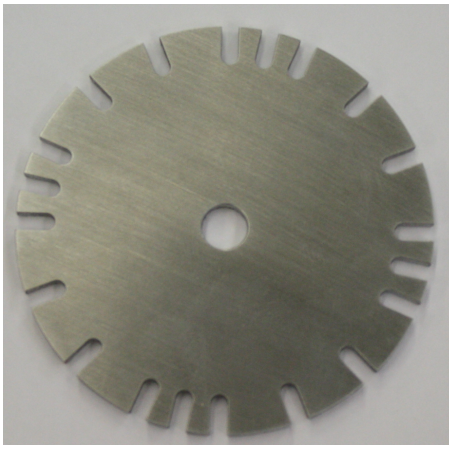

Figure 11: Photo of the aluminium cap.

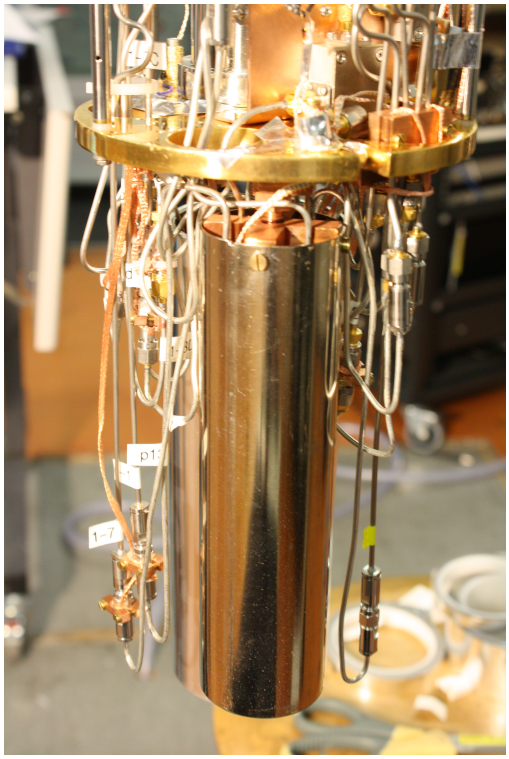

Figure 12: Photo of the shield as it is mounted onto the cryostat.

5. Measurement techniques

The different properties of the qubit can be detected by using several measurement schemes. A detailed description of them can be found for example in [10]. Here only the basic ideas of how to measure the decoherence times are presented.

In a first step the frequency of the resonator ν_{res} is determined by measuring the transmission through the resonator as a function of frequency. The resulting spectrum is fitted with a Lorentzian and is maximal at the resonator frequency.

With this information the frequency ν_{qubit} of the qubit can be extracted, by measuring the transmission of a microwave signal at resonance frequency ν_{res} through the resonator, as a function of the frequency of another microwave signal applied as a gate voltage. When the frequency of the latter is at ν_{qubit} the qubit will get partially excited. Due to the coupling of the qubit to the photons in the line resonator, the resonance frequency ν_{res} will be shifted. This appears as a minimum in the transmission through the resonator.

In a third step, a pulse with frequency ν_{qubit} is applied as a gate voltage. Then the population of the excited state is determined as a function of the pulse length at constant amplitude by measuring the transmission of a signal at frequency ν_{res} through the resonator after the pulse has been applied. The probability to measure an excited state will oscillate as a function of the length of the pulse. This effect is called Rabi oscillation. Out of this data, the length and amplitude of a pulse which excites the qubit from the ground state to the excited state (π-pulse) as well as length and amplitude of a pulse which excites the qubit to a state where ground and excited state are equally probable ($\pi/2$-pulse) can be obtained.

Knowing how to excite the qubit it is now easy to measure the energy relaxation time T_1: The qubit is excited with a π-pulse out of the ground state and then measured after a time delay τ. As in the time τ the qubit decays with the rate $1/T_1$, the probability to be in the excited state decreases exponentially $p_{|e\rangle}(\tau) = e^{-\tau/T_1}$. Fitting this curve to the measured data gives T_1.

5.1. Measurement of the dephasing time

Finally it is possible to measure the dephasing time. This is done using the Ramsey method [17]. For this purpose the qubit is excited with a $\pi/2$-pulse. After a free evolution of a time τ a second $\pi/2$-pulse is applied and the state of the qubit is measured.

If the drive frequency is detuned from the qubit frequency by $\Delta\omega$ the probability to measure the qubit in the excited state $p_{|e\rangle}$ is then given by [18]

$$p_{|e\rangle} = \frac{1}{2} + \frac{\cos(\Delta\omega\tau)}{2}. \tag{5}$$

If random dephasing happens during the time τ, the probability to be in the excited state is changed. In average it is $\langle p_{|e\rangle}\rangle = \frac{1}{2}$. As you need to average over a lot of

measurements anyway, this can be combined with equation 5. For 1/f noise the total probability is

$$p_{|e\rangle} = \frac{1}{2} + \frac{e^{\frac{\tau}{T_2}}}{2} \cos\left(\Delta\omega\tau\right).$$

This can be fitted to the measurement data to extract T_2. Note that as this method averages over many single measurements the measured T_2 is only a lower boundary for the value of T_2 in a single measurement, see [10]. An example of measurement data for all these five measurement schemes mentioned here can be found in figure 13.

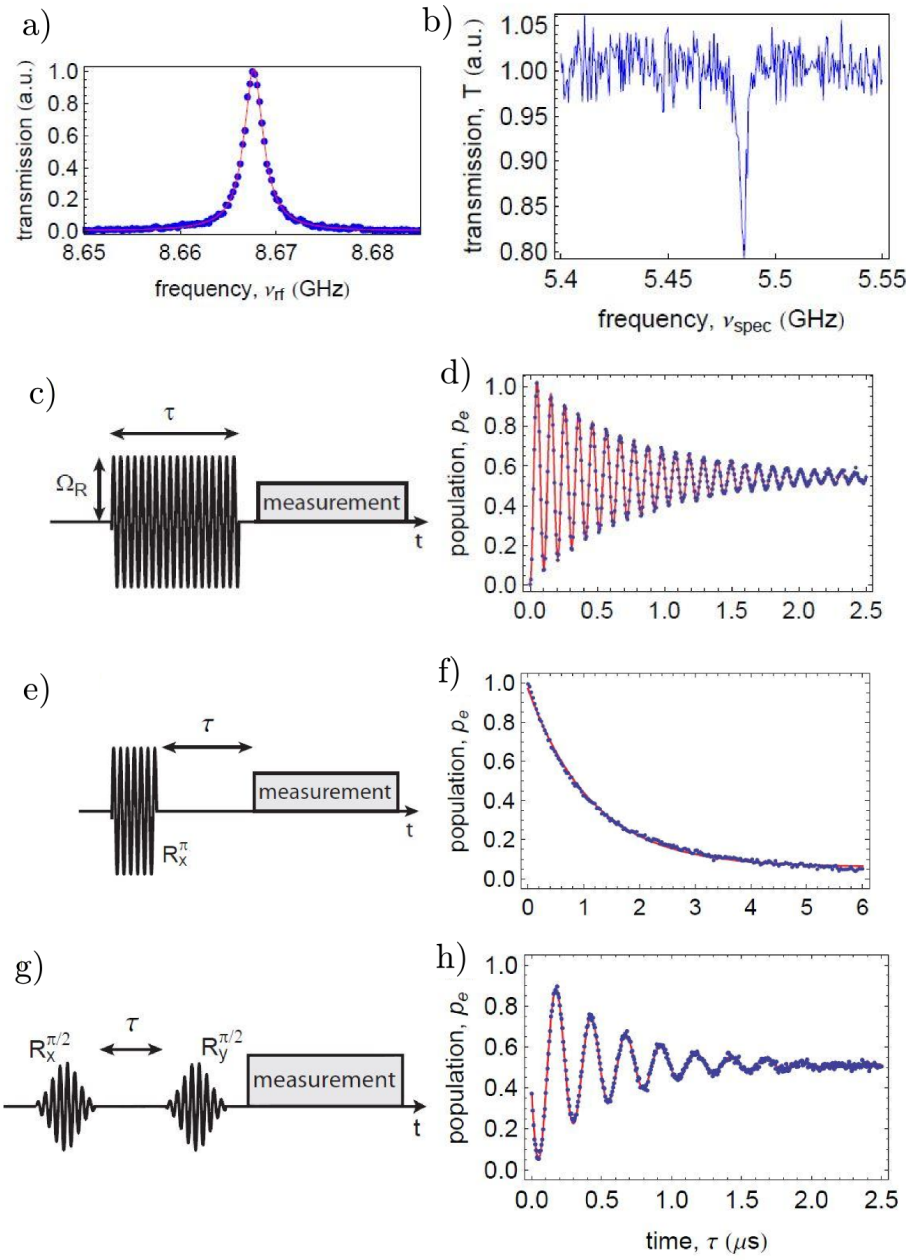

Figure 13: Overview of a decoherence measurement. a) resonator spectroscopy, b) qubit spectroscopy, c) & d) Rabi principle & measurement, e) & f) T_1 principle & measurement and g) & h) Ramsey principle & measurement. [10].

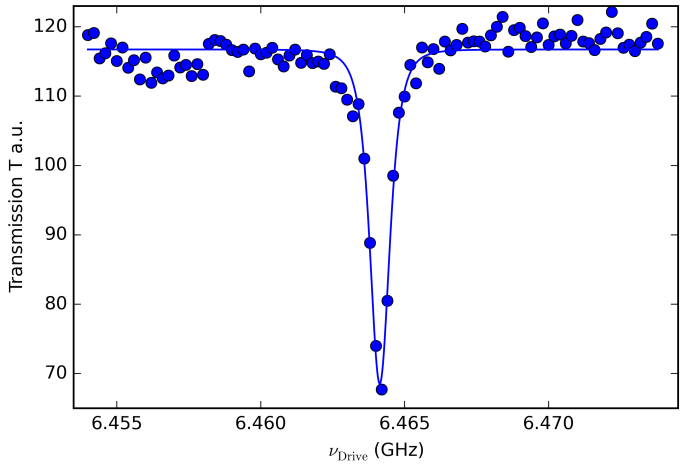

Figure 14: Transmission through the resonator as a function of the drive frequency. The line shows the Lorentzian which was fitted to determine the qubit frequency.

6. Results

6.1. Stability of the qubit frequency

To determine the stability of the qubit frequency, the transmission of the qubit has been measured as a function of the drive frequency approximately every 15 s over several hours. As described in section 5 and shown in figure 14 the qubit frequency can be obtained by fitting these measurements with a Lorentzian. Two such measurements have been analysed. The stability without a superconducting shield is shown in figure 15. Note that in addition to the qubit frequency its numerical derivative the drift velocity

$$v_{\mathrm{drift}} := \frac{\Delta \nu_{\mathrm{Qubit}}}{\Delta t}$$

is shown. The same for a measurement with the superconducting shield is found in figure 16. The average drift frequencies and the standard deviation of the drift frequencies are listed in table 1. Note that there is no improvement of these properties due to the new shield.

6.2. Dephasing time

As described in section 5.1 the dephasing time T_2 has been measured for different qubit frequencies.[7] Note that the dephasing time did not increase after the installation of the

[7] @ Markus: Where do the errorbars come from? From the fit?

	without shield	**with shield**
$\bar{v_{\text{drift}}} =$	$-16\,\text{Hz/s}$	$-16\,\text{Hz/s}$
$\sqrt{\bar{v_{\text{drift}}}^2 - \bar{v_{\text{drift}}}^2} =$	$3.2\,\text{kHz/s}$	$3.6\,\text{kHz/s}$

Table 1: Average and standard deviation of the drift velocity with and without the superconducting shield.

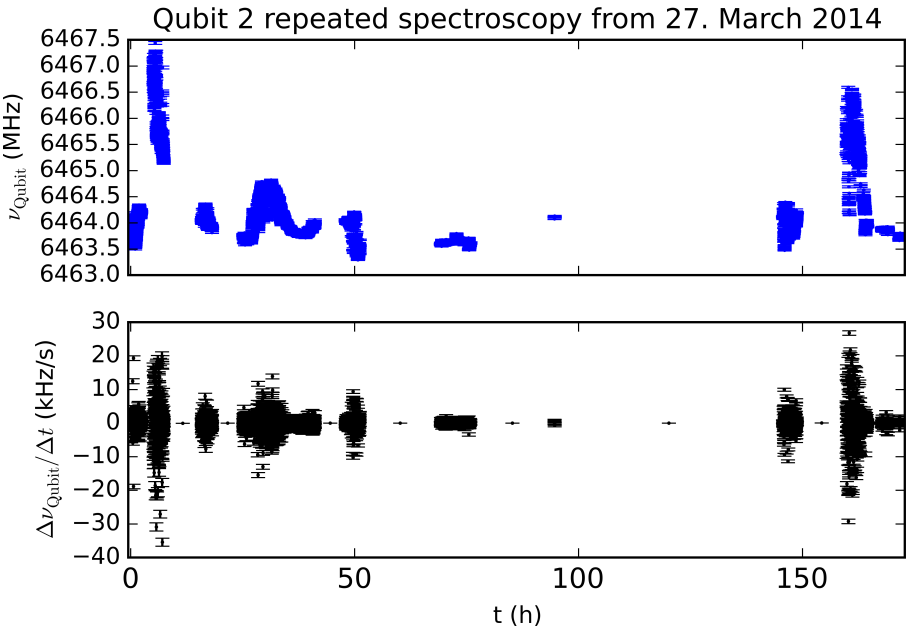

Figure 15: Time evolution and its derivative of the qubit frequency without a superconducting shield.

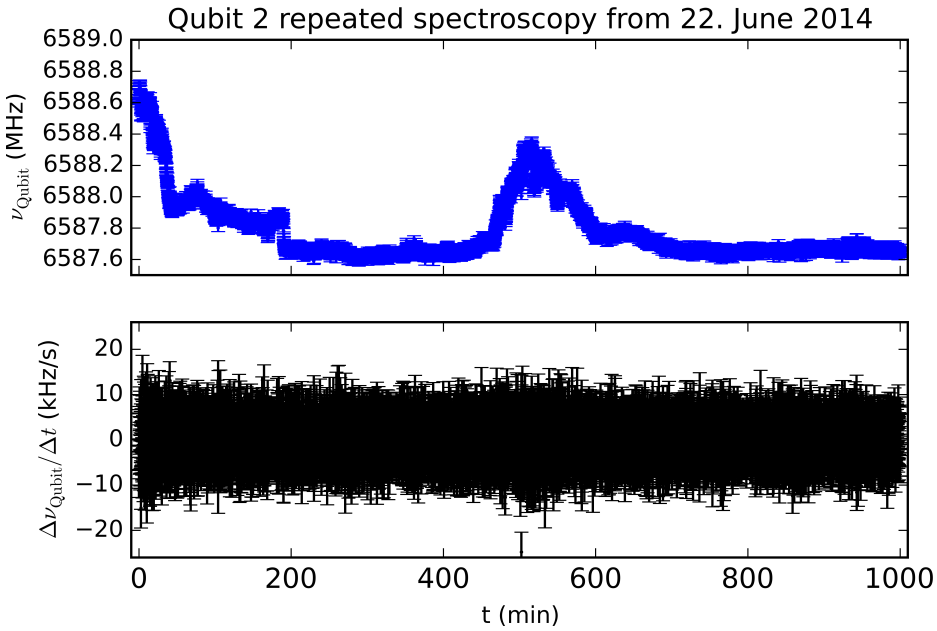

Figure 16: Time evolution and its derivative of the qubit frequency with a superconducting shield.

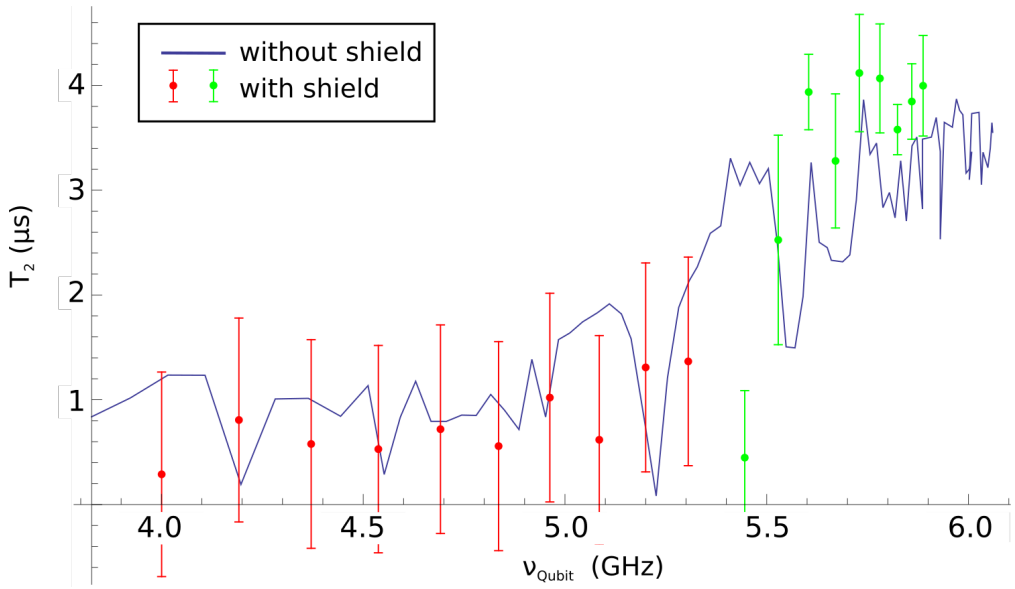

Figure 17: Dephasing time T_2 as a function of the qubit frequency, modified from [19].

new shield.

6.3. Initial flux offset

An additional quantity which allows to measure the influence of magnetic fields on the qubit is the flux through the loop, see figure 3. If there are no remanences in the environment of the qubit this quantity is exclusively given by external magnetic fields. In figure 18 this flux offset is shown from measurements over several years. There could be a slight improvement due to the new shield.

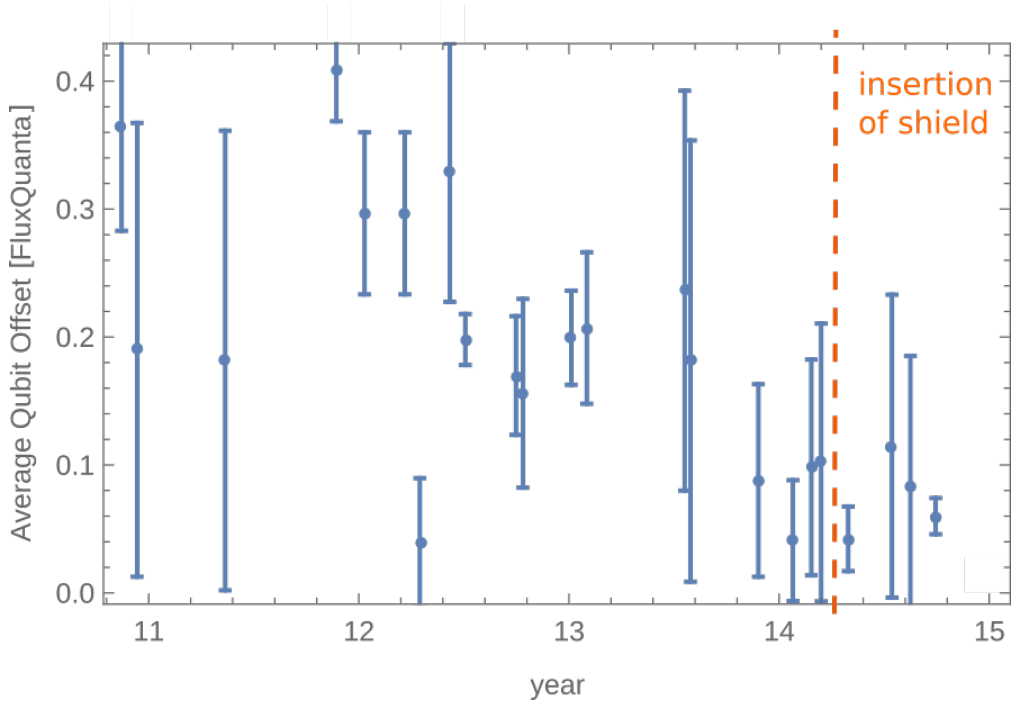

Figure 18: Flux offset from the ideal qubit frequency after cool-down, modified from [19].

7. Conclusion

A superconducting magnetic shield has been designed and produced out of aluminium. Simulations imply that it should improve the shielding of external magnetic fields by more than a factor of five hundred. However no measurable improvement could be detected in any of the analysed quantities. Neither the dephasing time nor the flux offset nor the stability of the qubit frequency improved after the shield had been installed.

Nevertheless this does not have to implicate that the simulation is incorrect. It could also be that all these properties are limited by other factors. Among others such factors could be noise on the flux lines or vibration of the coils used to generate the flux through the qubit. If they cause stronger magnetic fluctuations at the location of the qubit than the shielded external magnetic field no effect of a better shielding would be seen.

It is suggested to mount the cap the next time the wiring has to be adjusted, too. According to the simulation this should improve the shielding by another factor of five. In addition one should try to determine which effects are mainly causing the dephasing and the drift of the qubit frequency.[8] One could also try to check again whether there are no errors in the simulation. This could for example be done by changing the relative permeability of the superconductor to even smaller values and see if this changes the results of the simulation.

[8] @ Markus: How could this be done?

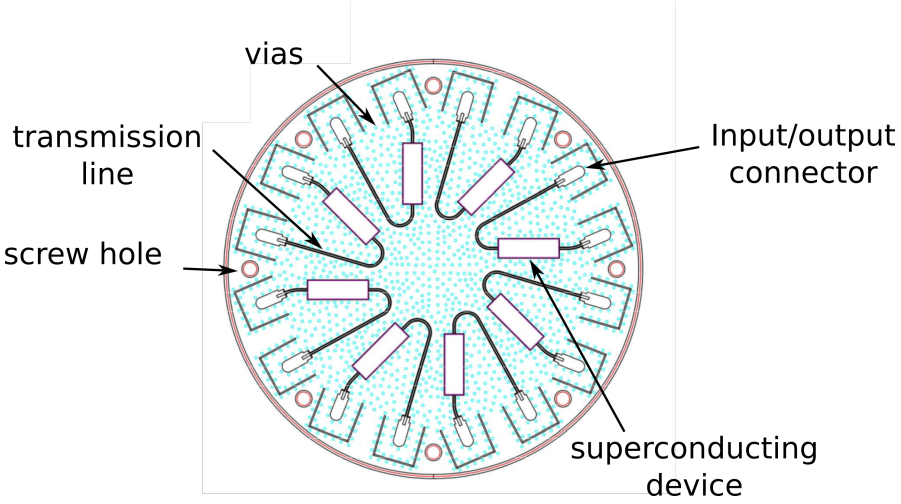

Figure 19: Components used in the PCB design, modified from [14].

Appendix A PCB designs and covers

As a part of the work in the lab, I designed new PCB geometries, as it was also done by [14], and the appropriate PCB covers. The latter consist of copper and are used to suppress unwanted cavity resonances, see [20, 21]. The components of a PCB are indicated in figure 19. In Fig. 20 the new PCB designs are shown. They were drawn with the commercial computer program *Atodesk Auto CAD 2014*. Note that as in [14] the radius of all the bends is at least three times the width of the transmission line. The aim was to design PCBs which allow either to place more superconducting devices than previous designs or to enable the measurement of the transmission through several superconducting devices. A corresponding PCB cover is shown in Fig. 21. Note that neither the PCBs nor the covers have been produced.

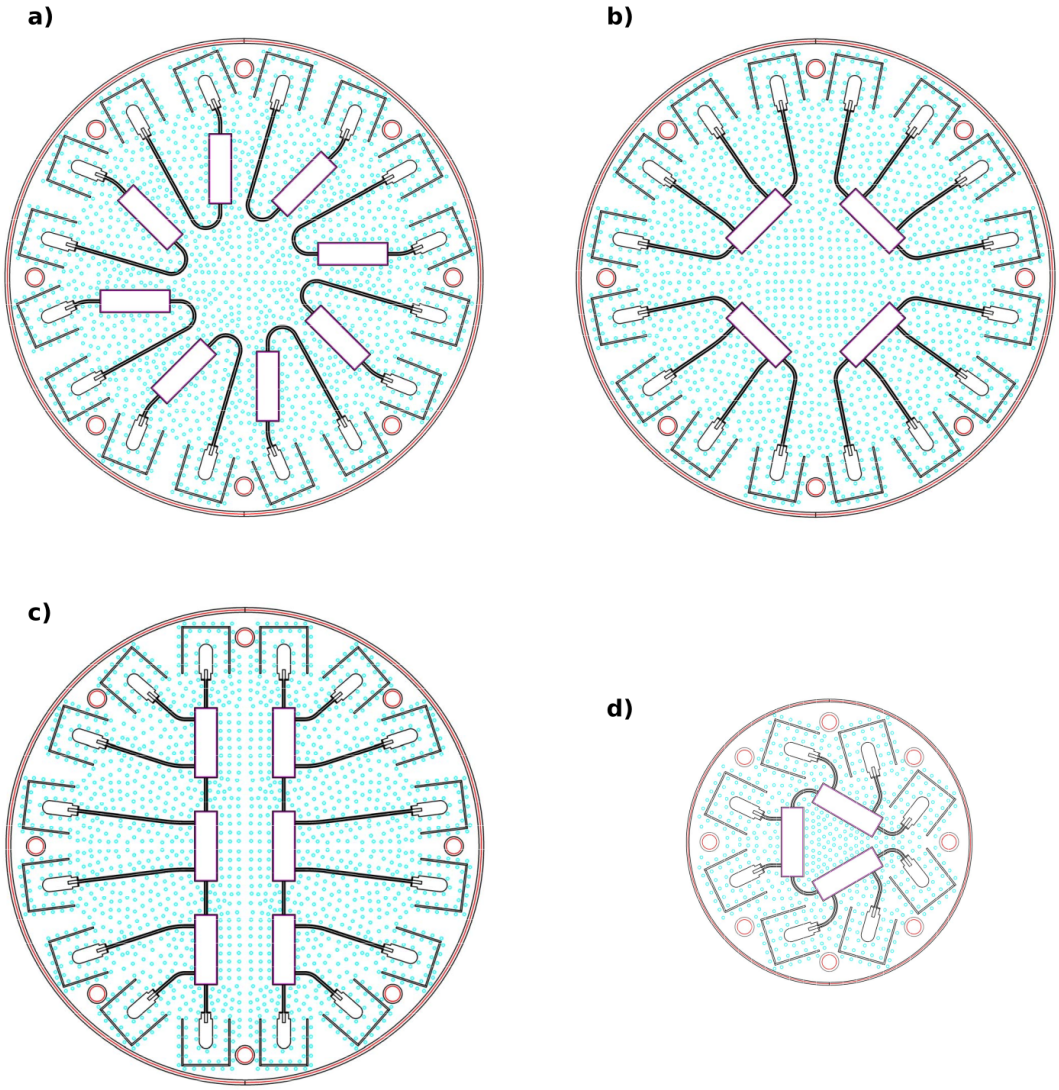

Figure 20: New PCB designs for the 16-port holder (**a)-c)**) and for the 8-port holder **d)**.

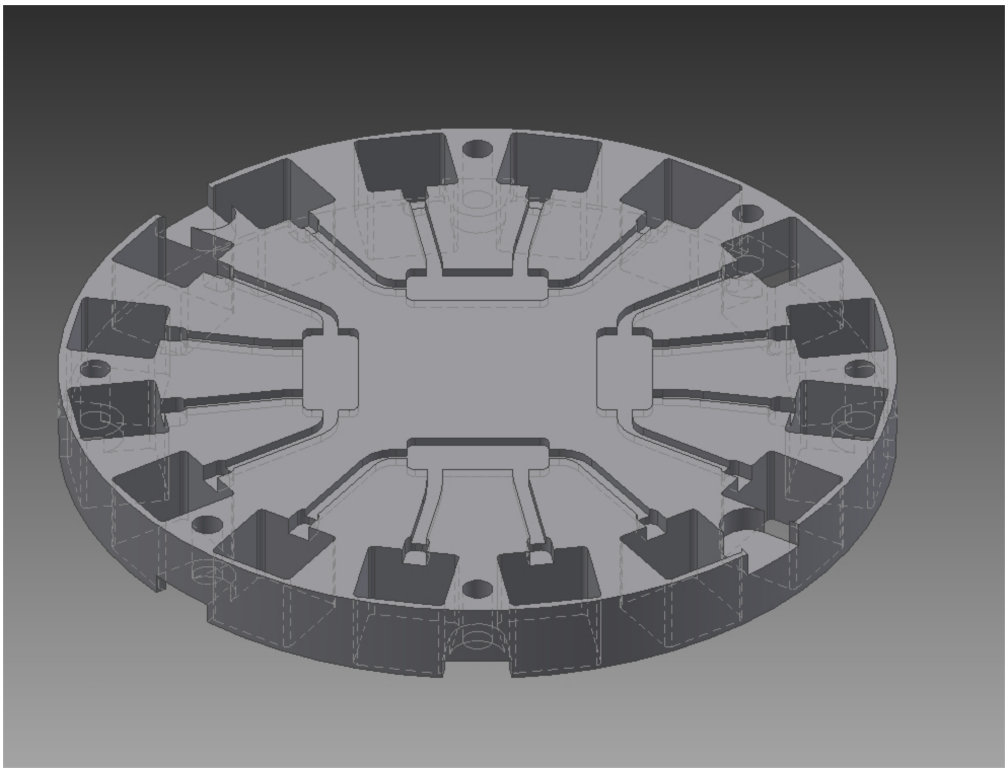

Figure 21: The PCB cover corresponding to the PCB in figure 20 b).

8. Acknowledgements

I would like to thank Prof. Dr. Andreas Wallraff for giving me the possibility to write my semester thesis in his group, Markus Oppliger for his supervision of my thesis and for analysing the T_2 as well as the flux offset data, Dr. Mintu Mondal for his supervision while Markus was absent and Yves Salathé for preparing a template file for the simulation.

9. Bibliography

References

[1] L. K. Grover, "A fast quantum mechanical algorithm for database search," in *Proceedings of the twenty-eighth annual ACM symposium on Theory of computing*, (Philadelphia, Pennsylvania, United States), pp. 212–219, ACM, 1996.

[2] J. Koch, T. M. Yu, J. Gambetta, A. A. Houck, D. I. Schuster, J. Majer, A. Blais, M. H. Devoret, S. M. Girvin, and R. J. Schoelkopf, "Charge-insensitive qubit design derived from the Cooper pair box," *Phys. Rev. A*, vol. 76, no. 4, p. 042319, 2007.

[3] S. Celozzi, R. Araneo, and G. Lovat, *Electromagnetic Shielding*. John Wiley & Sons, Inc., 2008.

[4] M. Tinkham, *Introduction to Superconductivity*. McGraw-Hill International Editions, 1996.

[5] H. Ibach and H. Lüth, *Solid-State Physics*. Springer Berlin Heidelberg, 4 ed., 2009.

[6] M. Peterer, "Investigating the suppression of external sources of decoherence in transmon qubits," Master's thesis, ETH Zurich, 06 2012.

[7] A. Cottet, *Implementation of a quantum bit in a superconducting circuit*. PhD thesis, Université Paris 6, 2002.

[8] D. I. Schuster, *Circuit Quantum Electrodynamics*. PhD thesis, Yale University, 2007.

[9] V. Bouchiat, D. Vion, P. Joyez, D. Esteve, and M. H. Devoret, "Quantum coherence with a single Cooper pair," *Phys. Scr.*, vol. T76, pp. 165–170, 1998.

[10] M. Baur, *Realizing quantum gates and algorithms with three superconducting qubits*. PhD thesis, ETH Zurich, 03 2012.

[11] S. Haroche and J.-M. Raimond, *Exploring the Quantum: Atoms, Cavities, and Photons*. Oxford University Press, New York, USA, 2006.

[12] J. Fink, *Quantum nonlinearities in strong coupling circuit QED*. PhD thesis, ETH Zurich, 10 2010.

[13] D. M. Pozar, *Microwave Engineering*. Addison-Wesley Publishing Company, 1993.

[14] S. Schmidlin, "Design and characterization of microwave printed circuit boards for circuit qed experiments," Master's thesis, ETH Zurich, 09 2008.

[15] R. N. Simons, *Coplanar waveguide circuits, components and systems.* Wiley Series in Microwave and Optical Engineerging, Wiley Inter-Science, 2001.

[16] D. U. Gubser and A. W. Webb, "High-pressure effects on the superconducting transition temperature of aluminum," *Phys. Rev. Lett.*, vol. 35, pp. 104–107, Jul 1975.

[17] N. F. Ramsey, "A molecular beam resonance method with separated oscillating fields," *Phys. Rev.*, vol. 78, pp. 695–699, Jun 1950.

[18] R. Bianchetti, *Control and readout of a superconducting artificial atom.* PhD thesis, ETH Zurich, 08 2010.

[19] Quantum Device Laboratory, ETH Zurich, internal communication.

[20] Y. Liu, "Implementation and characterization of 16-port devices in circuit quantum electrodynamics," Master's thesis, ETH Zurich, 04 2012.

[21] S. Marx, "Optimization of the microwave properties of a cryostat sample holder," Master's thesis, ETH Zurich, 07 2009.

ETH

Eidgenössische Technische Hochschule Zürich
Swiss Federal Institute of Technology Zurich

Declaration of originality

The signed declaration of originality is a component of every semester paper, Bachelor's thesis, Master's thesis and any other degree paper undertaken during the course of studies, including the respective electronic versions.

Lecturers may also require a declaration of originality for other written papers compiled for their courses.

I hereby confirm that I am the sole author of the written work here enclosed and that I have compiled it in my own words. Parts excepted are corrections of form and content by the supervisor.

Title of work (in block letters):

Design of a superconducting magnetic shield

Authored by (in block letters):

For papers written by groups the names of all authors are required.

Name(s):	**First name(s):**
Krieger	Jonas

With my signature I confirm that

- I have committed none of the forms of plagiarism described in the 'Citation etiquette' information sheet.
- I have documented all methods, data and processes truthfully.
- I have not manipulated any data.
- I have mentioned all persons who were significant facilitators of the work.

I am aware that the work may be screened electronically for plagiarism.

Place, date	**Signature(s)**
Zurich, 1.12.15	J. Krieger

For papers written by groups the names of all authors are required. Their signatures collectively guarantee the entire content of the written paper.